



Impact of receiver architecture on small satellite optical link in the presence of pointing jitter

IMAM Uz ZAMAN*  AND OZDAL BOYRAZ 

Department of Electrical Engineering and Computer Science in the University of California, Irvine, California 92697, USA

*Corresponding author: zamani@uci.edu

Received 3 September 2020; revised 12 October 2020; accepted 12 October 2020; posted 14 October 2020 (Doc. ID 409144); published 10 November 2020

The pointing jitter originated from the random mechanical vibration of the optical platform and the noise associated with the optomechanical sensor system unquestionably deteriorate the performance of the inter-satellite optical link. The impact of the jitter changes significantly with the receiver architecture. In this paper, we present a mathematical model to investigate the link performance in the presence of angular pointing jitters for different receiver architectures. Alongside the statistical pointing error model, the derived model incorporates key receiver design parameters such as detector radius, receiver aperture size, f -number of the lens system, and beam compression ratio to study the impact of receiver architecture on the pointing jitter. As an example, a CubeSat optical receiver is analyzed. We show that by careful selection of beam compression ratio and f -number, more than 5 orders of magnitude bit error rate improvement is achievable even at large pointing error. © 2020 Optical Society of America

<https://doi.org/10.1364/AO.409144>

1. INTRODUCTION

Small satellite technology continues to evolve to tackle more advanced and challenging space missions. The realization of a small satellite constellation facilitated by high-speed optical cross-link is being investigated to ensure the success of such missions [1–3]. One of the major challenges of an inter-satellite optical link (ISOL) is the necessity of the complex pointing, acquisition, and tracking (PAT) system. A well-engineered PAT mechanism is crucial in achieving maximum connectivity in a constellation where every satellite expects to sustain multiple data communication links simultaneously as shown in Fig. 1 [4,5]. The state-of-the-art ISOL usually operates in the presence of random angular pointing error (also known as pointing jitter). This pointing error arises primarily from the noise associated with the tracking sensors, the disturbance originated from the mechanical vibration, and the base motion of the satellites [6–8]. As a result, ISOL suffers from performance degradation. Up to date, several analytical models have been presented to understand the impact of pointing jitter on the performance of the digital and analog optical links [9,10]. In addition, authors studied the impact of random pointing and tracking error on coherent and incoherent optical satellite links in [11]. Several other works also investigated the performance degradation of the optical link due to the pointing jitters [6,12,13]. The main focus of the majority of these works was given toward the modeling of the nature of pointing jitters and, therefore, to estimate the overall link performance in terms of bit error rate

(BER) or bit error probability (BEP). However, the effect of the receiver architecture on the communication performance in the presence of pointing jitter is yet to be studied. Since the receiver architecture plays a critical role in the ISOL's immunity to the random pointing error, it is desirable to have an analytical study that facilitates a quick estimation of the link performance by using realistic receiver architecture parameters.

In this paper, we present a complete analytical model that incorporates both the receiver architecture parameters and statistical distribution of the pointing errors. In particular, we derive a mathematical performance model of a direct detection optical receiver to analyze the effect of receiver design parameters on the link immunity to the pointing jitters. The presented analytical model includes key receiver design parameters, such as detector radius, receiver aperture size, f -number of the focusing lens (FL) system, the beam compression ratio of the telescope, and the aberration parameter. Both instantaneous and average link performances are analyzed and presented using the derived model. As a case study, a CubeSat direct detection optical receiver is being studied. We show that by optimizing the beam compression ratio and minimizing the optical aberrations of the telescope more than 3 orders of magnitude BER improvement can be realized in a given ISOL. Moreover, our study indicates that 6 orders of magnitude BER improvement is realizable for a given ISOL by designing a receiver system with optimal selection of telescope beam compression ratio, f -number of the focusing system, and aberration parameter. Hence, the

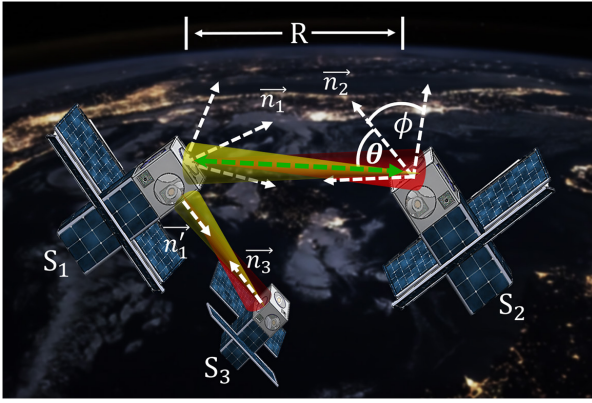


Fig. 1. Free space optical communication in a satellite constellation.

presented study facilitates the selection of the optimum design parameters for the best performance in the presence of random pointing errors.

2. STATISTICAL MODEL OF POINTING JITTERS AND THE EFFECT OF RECEIVER ARCHITECTURE ON PERFORMANCE

A. Model of Pointing Jitters and Receiver Architecture

The pointing errors depends on the electrical noises in the PAT sensors and the mechanical vibrations that couple to optical subsystems. The fundamental expression of the tracking sensor noise $\sigma_{\theta S}$ (standard deviation) has been studied before, and it has been expressed in terms slope factor of the transfer function ζ , which is a function of signal-to-noise ratio (SNR) S/N of the system, $\sigma_{\theta S} = \frac{1}{\sqrt{\zeta(S/N)}}$ [14]. Mechanical vibrations cause pointing error $\sigma_{\theta M}$ that can be modeled as $\sigma_{\theta M}^2 = \frac{1}{2\pi} \int S_{\theta}(\omega) |1 - H_T(\omega)|^2 d\omega$, where $S_{\theta}(\omega)$ is the power spectral density of the mechanical noise and $H_T(\omega)$ is the closed loop transfer function of the spatial tracking loop [11]. The combined effect of the electrical noise in PAT sensors and mechanical vibrations creates elevation and azimuth pointing angle errors. The probability density function (PDF) of both the elevation pointing error θ_{ET} and azimuth pointing error θ_{AT} has been modeled as normal distribution as $p(\theta_{ET}) = \frac{1}{\sqrt{2\pi\sigma_E^2}} \exp\left(-\frac{\theta_{ET}^2}{2\sigma_E^2}\right)$ and $p(\theta_{AT}) = \frac{1}{\sqrt{2\pi\sigma_A^2}} \exp\left(-\frac{\theta_{AT}^2}{2\sigma_A^2}\right)$, respectively [9,11]. Here, σ_E^2 and σ_A^2 represent the variance of the elevation and the azimuth pointing error, respectively. Assuming the distribution of θ_{ET} and θ_{AT} are independent, but alike, the PDF of the radial pointing error θ_T ($\theta_T^2 = \theta_{ET}^2 + \theta_{AT}^2$) is a Rayleigh distribution that can be expressed in terms of the variance of the radial pointing error σ_T^2 [9,11], $p(\theta_T) = \frac{\theta_T}{\sigma_T^2} \exp\left(-\frac{\theta_T^2}{2\sigma_T^2}\right)$. Due to the radial symmetry, we assume $\sigma_T = \sigma_A = \sigma_E$ [12,15]. The pointing jitters can affect the communication performance, especially at a large angle of incidence (AOI) θ as shown in Fig. 1. The initial communication link between the transmitter and the receiver is usually established with the help of ephemerides data

and advanced PAT system [16]. The transmitter and receiver usually achieve mutual line of sight tracking of each other by body pointing, coarse pointing, and fine pointing mechanisms [17–19]. However, due to the uncertainty of the satellite positions and the limited resolution of the PAT systems, θ can be significantly large between certain satellites in a constellation. For instance, in Fig. 1, a large AOI θ exists between S_1 and S_2 as the transmit beam of S_1 creates a large angle with respect to the receiver normal \vec{n}_2 . In contrast, a smaller θ exists between S_1 and S_3 since the transmit beam of S_1 aligns well with the receiver normal of S_3 (\vec{n}_3). For effective long-distance data communication, the AOI needs to be smaller than the receiver's field of view (FOV) ϕ , i.e., $\theta < \phi$. The instantaneous AOI at the receiver optical aperture can be written as $\theta_i = \theta + \theta_T$. For a given θ , the instantaneous received optical power by the receiver aperture $P_{rcv}(\theta_T)$ can be estimated from Friis transmission equation [20],

$$P_{rcv}(\theta_T) = P_T G_T G_R \alpha_T \alpha_R L_p \left(\frac{\lambda}{4\pi R}\right)^2 L_{PJ}(\theta_T). \quad (1)$$

Here, P_T , G_T , G_R , L_p , λ , R , α_T , and α_R represent average transmit power, transmit antenna gain, receiver antenna gain, pointing loss, operating wavelength, communication range, transmitter feeder loss, and receiver plumbing loss, respectively. The loss due to random pointing jitter $L_{PJ}(\theta_T)$ can be given by [11], $L_{PJ}(\theta_T) = \exp(-G_T \theta_T^2)$. Assuming θ varies much slower than the pointing jitter θ_T , the loss related to θ is lumped into the pointing loss L_p in the above-mentioned range equation. Hence, the instantaneous signal photo current $i_{PD}(\theta, \theta_T, \mathbb{S})$ depends on the receiver architecture that can be expressed in terms of the responsivity of the detector R_λ , the intrinsic gain of the photodetector G , and the performance degradation factor $K(\theta, \theta_T, \mathbb{S})$. Here, the performance degradation factor is determined by a set of receiver design parameters $\mathbb{S} = \{\text{aperture size, detector size, lens focal length, etc.}\}$,

$$i_{PD}(\theta, \theta_T, \mathbb{S}) = R_\lambda G P_{rcv}(\theta_T) \cdot K(\theta, \theta_T, \mathbb{S}). \quad (2)$$

The major causes of the performance degradation factor are random beam walk-off at the detector plane $\eta_{BO}(\theta, \theta_T, \mathbb{S})$, angle dependent detector responsivity $\eta_\lambda(\theta, \theta_T)$, reflection due to anti-reflection (AR) coating $\eta_{AR}(\theta, \theta_T)$, and free space to focusing lens (FL) coupling efficiency $\eta_C(\mathbb{A})$ ($\mathbb{A} \subset \mathbb{S}$). Hence, the performance degradation factor can be expressed as

$$K(\theta, \theta_T, \mathbb{S}) = \eta_{BO}(\theta, \theta_T, \mathbb{S}) \eta_{AR}(\theta, \theta_T) \eta_\lambda(\theta, \theta_T) \eta_C(\mathbb{A}). \quad (3)$$

In a high-speed free space communication system, due to the wavefront error of the received beam and the aberrations in the optical system, the focal spot size of the received beam is usually comparable to the active area of the high-speed detectors. Hence, in the presence of pointing jitter, the random beam walk-off at the detector plane becomes a dominant degradation factor. The performance degradation factor in the free space direct detection system can therefore be simplified and written as $K(\theta, \theta_T, \mathbb{S}) \approx \eta_{BO}(\theta, \theta_T, \mathbb{S}) \eta_C(\mathbb{A})$. Assuming the photodetector's radius r_d is close to but larger than the focal spot radius r_f , i.e., $r_d > r_f(d_B, f, \xi)$, the radial displacement of the focal spot center from the detector center $\rho(\kappa\theta, \kappa\theta_T)$, angle magnification factor of the receiver telescope κ , and $\theta < \phi$, the $K(\theta, \theta_T, \mathbb{S})$ can be approximated as

$$\begin{aligned}
 K(\theta, \theta_T, \mathbb{S}) &\approx \frac{0.318\eta_C(\mathbb{A})}{r_f(d_B, f, \xi)^2} (r_f(d_B, f, \xi)^2 \cos^{-1} \left(\frac{\gamma_2}{r_f} \right) \\
 &+ r_d^2 \cos^{-1} \left(\frac{\gamma_1}{r_d} \right) - \gamma_1 \sqrt{r_d^2 - \gamma_1^2} \\
 &- \gamma_2 \sqrt{r_f(d_B, f, \xi)^2 - \gamma_2^2}), \\
 &\approx \eta_C(\mathbb{A}) \quad \text{if } \rho(\kappa\theta, \kappa\theta_T) < r_d - r_f, \\
 &\approx 0 \quad \text{if } \rho(\kappa\theta, \kappa\theta_T) > r_d + r_f,
 \end{aligned} \tag{4}$$

$$\gamma_1 = \frac{r_d^2 - r_f(d_B, f, \xi)^2 + \rho(\kappa\theta, \kappa\theta_T)^2}{2\rho(\kappa\theta, \kappa\theta_T)},$$

$$\gamma_2 = \frac{r_f(d_B, f, \xi)^2 - r_d^2 + \rho(\kappa\theta, \kappa\theta_T)^2}{2\rho(\kappa\theta, \kappa\theta_T)}.$$

The focal spot radius $r_f(d_B, f, \xi)$ can be approximated from the beam diameter d_B , the beam mode quality M , and the focal length of the FL f and is given by $r_f(d_B, f, \xi) \approx 0.64M^2\lambda \frac{f}{d_B} + \xi \left(\frac{d_B^3}{2f^2} \right)$. The aberration factor ξ of the lens system depends on the materials of optical lenses, the curvature of the lens surfaces, and the receiver lens system design. A detail Gaussian beam propagation simulation or experimental validation is required to approximate ξ for a given optical system. For instance, ξ of a singlet plano-convex lens made from N-BK7 glass can be estimated by detail optical simulations (in Zemax) as $\xi = 0.1943 + 0.00202d_B - 0.000798f$. In this model, the numerical values of d_B (in mm) and f (in mm) need to be used to estimate the unit-less parameter ξ . Assuming θ is well controlled by the PAT system over the considered time duration to analyze the impact of the pointing jitter, the average SNR (SNR_{avg}) can be estimated from the instantaneous received power, the instantaneous noise power $\sigma_N^2(\theta, \theta_T)$, and σ_T as

$$\begin{aligned}
 \text{SNR}_{\text{avg}} &= R_\lambda^2 G^2 \int_0^\infty \frac{P_{\text{rcv}}(\theta_T)^2 K(\theta, \theta_T, \mathbb{S})^2}{\sigma_N^2(\theta, \theta_T)} \\
 &\cdot \frac{\theta_T}{\sigma_T^2} \exp \left(-\frac{\theta_T^2}{2\sigma_T^2} \right) d\theta_T.
 \end{aligned} \tag{5}$$

Considering a communication system that receives a pulsed light with a duty cycle D and an extinction ratio r_{ex} in a direct detection method, the instantaneous signal current for bits 1 can be expressed as $i_{pD-1}(\theta, \theta_T, \mathbb{S}) = \gamma \cdot i_{pD}(\theta, \theta_T, \mathbb{S})$. Similarly, the instantaneous signal current for bits 0 is given as $i_{pD-0}(\theta, \theta_T, \mathbb{S}) = \gamma r_{\text{ex}} i_{pD}(\theta, \theta_T, \mathbb{S})$. Here, $\gamma = \frac{1}{D(1-r_{\text{ex}})+r_{\text{ex}}}$. The instantaneous noise variances σ_{N-1}^2 (for 1) and σ_{N-0}^2 (for 0) are a function of signal currents, receiver dark current I_d , excess noise factor F_A , and the thermal noise σ_{TH}^2 . The noise variances can be expressed as

$$\begin{aligned}
 \sigma_{N-1}^2(\theta, \theta_T, \mathbb{S}) &= 2qF_A(i_{pD-1}(\theta, \theta_T, \mathbb{S}) + G^2 I_d) \Delta\nu + \sigma_{\text{TH}}^2, \\
 \sigma_{N-0}^2(\theta, \theta_T, \mathbb{S}) &= 2qF_A(i_{pD-0}(\theta, \theta_T, \mathbb{S}) + G^2 I_d) \Delta\nu + \sigma_{\text{TH}}^2.
 \end{aligned} \tag{6}$$

Here, q is the elementary charge. Consequently, the instantaneous Gaussian- Q function can be written as $Q(\theta, \theta_T, \mathbb{S}) = \frac{i_{pD-1}(\theta, \theta_T, \mathbb{S}) - i_{pD-0}(\theta, \theta_T, \mathbb{S})}{\sigma_{N-1}(\theta, \theta_T, \mathbb{S}) + \sigma_{N-0}(\theta, \theta_T, \mathbb{S})}$ [21]. Therefore, for a given θ and \mathbb{S} , the instantaneous error probability can be calculated from $Q(\theta, \theta_T, \mathbb{S})$,

$$p_e(\theta_T) \approx \frac{1}{2} \cdot \text{erfc} \left(\frac{Q(\theta, \theta_T, \mathbb{S})}{\sqrt{2}} \right). \tag{7}$$

Finally, the system BER can be obtained by averaging the instantaneous BEP $p_e(\theta_T)$ and can be written as

$$\text{BER} = \int_0^\infty p_e(\theta_T) p(\theta_T) d\theta_T. \tag{8}$$

B. Model of a Sample Direct Detection Receiver

The general formulation presented in the previous section can be modified according to a specific receiver architecture. As an illustration, here, we present the performance estimation model of a sample direct detection receiver in a small satellite platform as shown in Fig. 2.

The sample receiver has a clear aperture diameter of d_R , and the telescope beam compressor reduces the beam diameter to d_B . In a long-distance communication, we can assume a plane wave illuminates the entire receiver aperture. Therefore, the beam compression ratio m_T can be defined as $m_T^{-1} = \frac{d_B}{d_R}$ and $\kappa \approx m_T$ in Eq. (4). The detector diameter and the focal spot diameter are denoted as $2r_d$ and $2r_f$, respectively. A beam sampler (BS) is usually used to sample a fraction beam for the quadrant detector (QD) to facilitate the pointing and tracking mechanisms [2]. In Fig. 2, the on-axis received beam is shown as a solid blue line, and the off-axis received beam is shown as a dashed orange line. All angles are measured w.r.t. the direction normal to the receiver \vec{n} . Besides, θ_T is the instantaneous pointing error, and θ_r is the instantaneous total angular variation of the compressed beam. θ_r can be expressed as $\theta_r = m_T(\theta + \theta_T)$. Finally, a FL of diameter d_{FL} focuses the beam on the detector (D). To simplify the model, we lump the impact of optical aberration in ξ . Hence, the coupling efficiency is approximated as $\eta_C(\mathbb{A}) = \left(\frac{m_T d_{\text{FL}}}{d_R} \right)^2$ if $m_T d_{\text{FL}} \leq d_R$; otherwise, $\eta_C \approx 1.0$. $\mathbb{A} = \{m_T, d_R, d_{\text{FL}}\}$. The radial displacement of the center of the focal spot from the center of the detector can be expressed as $\rho(\kappa\theta, \kappa\theta_T) \approx f m_T(\theta + \theta_T)$. Under small-angle approximation, the instantaneous performance degradation factor of

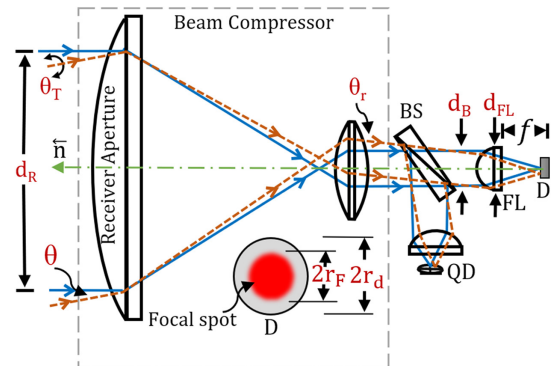


Fig. 2. Sample direct detection optical receiver.

the sample receiver architecture $K_s(\theta, \theta_T, \mathbb{S})$ is derived from Eq. (4) and is given by

$$\begin{aligned}
 K_s(\theta, \theta_T, \mathbb{S}) &= \frac{\eta_C(\text{A})}{\pi} \\
 &\times \sec^{-1} \left(\frac{2fr_fm_T(\theta + \theta_T)}{-r_d^2 + r_f^2 + f^2m_T^2(\theta + \theta_T)^2} \right) \\
 &+ \frac{\eta_C(\text{A})}{\pi} \left(\frac{r_d}{r_f} \right)^2 \\
 &\times \sec^{-1} \left(\frac{2fr_fm_T(\theta + \theta_T)}{r_d^2 - r_f^2 + f^2m_T^2(\theta + \theta_T)^2} \right) \\
 &- \frac{\theta_r f \eta_C(\text{A})}{\pi r_f^2} \left[r_d^2 - \frac{(r_d^2 - r_f^2 + f^2m_T^2(\theta + \theta_T)^2)^2}{4f^2m_T^2(\theta + \theta_T)^2} \right]^{1/2} \\
 &= \eta_C(\text{A}) \quad \text{if } fm_T(\theta + \theta_T) < r_d - r_f \\
 &= 0 \quad \text{if } fm_T(\theta + \theta_T) > r_d + r_f.
 \end{aligned} \tag{9}$$

Equation (9) reveals the effect of receiver design parameters, $\mathbb{S} = \{m_T, r_d, d_R, f, d_{\text{FL}}, \xi\}$, on the degradation factor. Depending on the random pointing jitter and the receiver parameters, K_s can vary between 0.0 and 1.0, $0 \leq K_s(\theta, \theta_T, \mathbb{S}) \leq 1$. Once we estimate the received power on the detector, the instantaneous BEP and the BER of the sample receiver can be calculated using Eqs. (7) and (8), respectively. Generally in a receiver design, $d_{\text{FL}} \geq d_B$; therefore, we can assume $\eta_C(\text{A}) \approx 1.0$. Additionally, assuming a Gaussian beam with $M^2 \approx 1.0$ and the incorporated FL has an f -number of N , the performance degradation factor expression in Eq. (9) can be simplified further and given as

$$\begin{aligned}
 &K_s(\theta_T, r_d, d_R, N, m_T, \xi, \tau) \\
 &\approx \frac{1}{\pi} \sec^{-1} \left(\frac{2ABNd_R}{B^2 + A^2N^2d_R^2 - r_d^2} \right) \\
 &- \frac{1}{B^2\pi} ANd_R \sqrt{r_d^2 - \frac{(-B^2 + A^2N^2d_R^2 + r_d^2)^2}{4A^2N^2d_R^2}} \\
 &+ \frac{r_d^2}{B^2\pi} \sec^{-1} \left(\frac{2ANd_Rr_d}{-B^2 + A^2N^2d_R^2 + r_d^2} \right) \\
 &\approx 1 \quad \text{if } N \left(\frac{\tau r_d}{N} + d_R\theta_T \right) < r_d - B \\
 &\approx 0 \quad \text{if } N \left(\frac{\tau r_d}{N} + d_R\theta_T \right) > r_d + B \\
 &A = \theta_T + \frac{\tau r_d}{d_R N} \quad \text{and} \quad B = 0.64N\lambda + \frac{d_R\xi}{2m_T N^2}. \tag{10}
 \end{aligned}$$

Here, τ is the ratio of the AOI to the receiver's FOV, i.e., $\tau = \frac{\theta}{\phi}$. The beam compression ratio m_T of the sample receiver architecture as shown in Fig. 2 is limited by the diffraction-limited focus spot size of the aperture lens and

the manufacturable optics. The diffraction-limited spot size (airy disk radius) after the aperture lens can be calculated from the focal length of the aperture lens f_R , and can be given as $r_a = \frac{0.64M^2\lambda f_R}{d_R}$. Hence, the realizable compression ratio of the sample telescope can be expressed as $m_T \ll \frac{d_R^2}{1.28M^2\lambda f_R}$.

3. PERFORMANCE ANALYSIS AND SIMULATION RESULTS

The link parameters and the receiver design parameters are summarized in Table 1. In our analyses, we consider values for each parameter that are typically used in the state-of-the-art systems based on a literature survey and manufacturer specifications [22–24]. Although the considered design parameters are pertinent to CubeSat omnidirectional optical link [4,24], all analyses apply to any satellite optical link with the appropriate design and link parameters.

A. Instantaneous Performance Degradation Analyses

Equation (10) reveals the dependence of the instantaneous performance degradation factor K_s on the detector size r_d , the receiver aperture size d_R , the N of the FL, the beam compression ratio m_T , the ratio of the AOI to the FOV τ , and the aggregated aberration factor ξ of the lens system. To demonstrate the instantaneous performance degradation, we choose an omnidirectional CubeSat platform [24] with a 15 mm receiver aperture, i.e., $d_R = 15.0$ mm and the instantaneous pointing error, $\theta_T = 0.5$ μrad . As $\theta_T \ll \tau\phi$, the effect of instantaneous θ_T is negligible on K_s . However, the distribution of θ_T significantly affects the average link performance as expected from Eqs. (5) and (8).

A sample analysis to demonstrate the dependence of K_s on τ and r_d (assuming $\xi = 0.15$) is presented in Fig. 3. Figures 3(a) and 3(b) show the performance degradation for $N = 2.0$ and $N = 3.0$, respectively. It can be seen from Fig. 3(a) that K_s drops

Table 1. Optical Link Parameters

| Parameters | Symbol | Value |
|-------------------------------------|------------------|-----------------------------|
| Modulation format | | OOK |
| Communication distance | R | 100.0 km |
| Transmit power | P_T | 1.0 W |
| Wavelength | λ | 1550 nm |
| Transmitter feeder loss | α_T | 2.0 dB |
| Receiver plumbing loss | α_R | 2.0 dB |
| Link pointing loss | L_P | 3.0 dB |
| Communication bandwidth | $\Delta\nu$ | 1.0 GHz |
| APD gain | G | 50 |
| APD responsivity | R_λ | 0.8 |
| APD noise equivalent power | NEP | 30.0 pW/ $\sqrt{\text{Hz}}$ |
| Average dark current | I_d | 15.0 nA |
| Excess noise factor | F_A | 2.0 |
| Detector size (diameter) | $2r_d$ | 0.2–0.5 mm |
| Transmit beam size (diameter) | d_T | 15.0 mm |
| Receiver aperture (diameter) | d_R | 15.0 mm |
| Received power (w/o pointing error) | P_{rcv} | −35.77 dBm |
| BER (w/o pointing errors) | | $\approx 2 \times 10^{-11}$ |

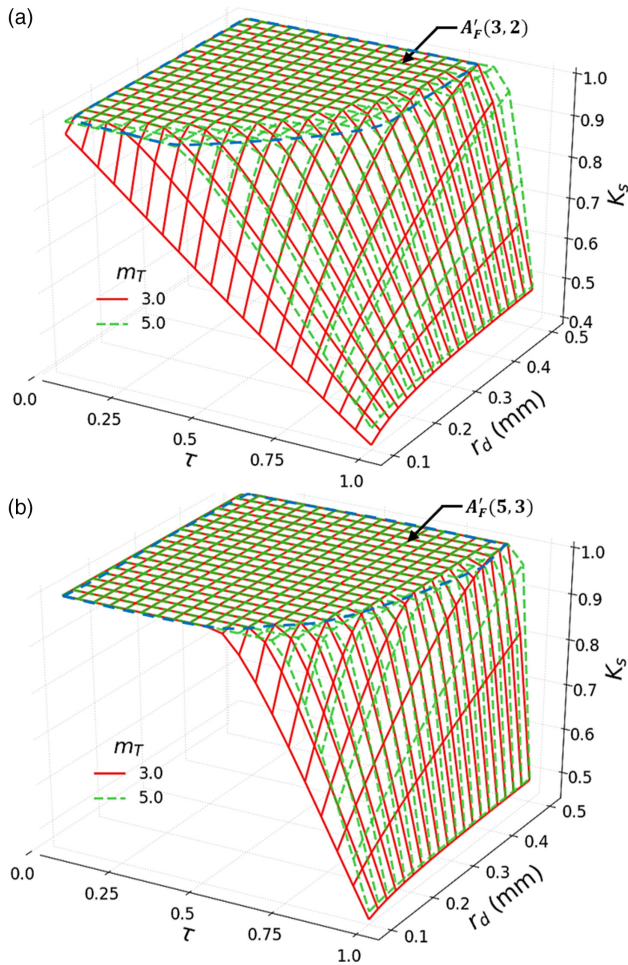


Fig. 3. Effect of τ and r_d on k_s for $m_T = \{3, 4\}$. (a) $N = 2.0$; (b) $N = 3.0$.

to 0.4 from 0.99 almost linearly within a range of $0 \leq \tau \leq 1$ for $r_d = 0.1$ mm and $m_T = 3.0$. On the contrary, for $r_d = 0.5$ mm and $m_T = 3.0$, K_s remains stable (close to 1.0) for $\tau \leq 0.81$. Hence, increasing r_d improves the receiver tolerance to τ for a given m_T , as expected. Further improvement of receivers' tolerance by increasing m_T is evident from Fig. 3(a). Although the angular variation increases due to the beam compression, i.e., $\theta_r \approx m_T \theta_i$, the impact of m_T can be counterbalanced by the FL parameters. The resultant beam walk-off at the detector plane is found to be $\rho \approx \zeta \theta_i N d_R$, where $\zeta = \frac{d_{FL}}{d_B}$. Besides, in an aberration limited optical receiver, $r_f \propto d_B^3 \propto 1/m_T^3$. Therefore, for a given aperture size, a larger m_T tends to create a smaller focal spot. As a result, the probability of beam clipping at the detector decreases due to lateral movement of focal spot that improves the achievable average SNR in the presence of pointing jitter. For example, if a beam compressor with $m_T = 5.0$ is incorporated, then K_s is close to 1.0 for $\tau \leq 0.43$ for $r_d = 0.1$ mm and K_s gradually decreases to 0.25 when τ approaches 1.0 as shown in Fig. 3(a).

A higher N also helps to make the receiver system less sensitive to pointing errors. For instance, it can be seen from Fig. 3(b) that for $m_T = 3.0$, $N = 3.0$, and $r_d = 0.1$ mm, K_s remains close to 1.0 for $\tau \leq 0.57$ and then gradually drops to 0.45

when τ gradually approaches to 1.0. Visually, the sensitivity of K_s on the design parameters can be compared based on the area of the quasi-flat region (relatively constant K_s region) A'_F of the plots where $K_s \geq 0.98$. It can be qualitatively realized that $A'_F(3, 2) < A'_F(5, 2) < A'_F(3, 3) < A'_F(5, 3)$. Here, $A'_F(m_T, N)$ represents the area of the quasi-flat region of the plots for given m_T and N as shown in Fig. 3. A larger A'_F implies higher immunity to incident angle errors. Therefore, we can say that among the considered combination of design parameters, the receiver system with $m_T = 3.0$ and $N = 2.0$ has the lowest immunity to pointing jitters, whereas the system with $m_T = 5.0$ and $N = 3.0$ demonstrates the highest immunity.

The effect of τ and ξ on the instantaneous performance degradation for two different detector radiuses, $r_d = \{0.1 \text{ mm}, 0.25 \text{ mm}\}$, is presented in Fig. 4. Figure 4(a) shows the impact of ξ and τ on K_s for $m_T = 3.0$ and $N = 3.0$. For instance, it can be seen from Fig. 4(a) that at $\xi = 0.15$ and $r_d = 0.25$ mm, the factor K_s is close to 1.0 for $\tau \leq 0.95$. In contrast, a 0.1 mm detector shows $K_s \geq 0.98$ for $\tau \leq 0.8$ at the same aberration, $\xi = 0.15$. It is also realizable from Fig. 4(a) that K_s can vary from 1.0 to 0.4 over the range $0.2 < \tau \leq 1.0$ based on the receiver parameters r_d and ξ . Evidently, a receiver with larger r_d is more immune to variation of τ and ξ . The

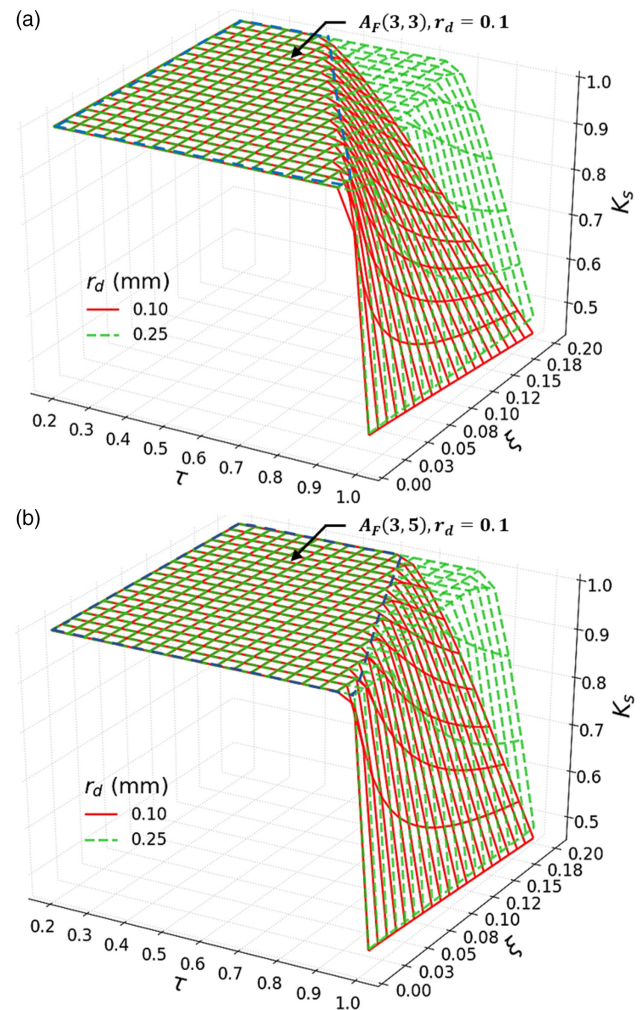


Fig. 4. Impact of τ and r_d on k_s for $r_d = \{0.1 \text{ mm}, 0.25 \text{ mm}\}$. (a) $N = 3.0$, $m_T = 3.0$; (b) $N = 3.0$, $m_T = 5.0$.

Table 2. Receiver's Instantaneous FOV (Half-Angle)

| r_d (mm) | N | ϕ (°) | r_d (mm) | N | ϕ (°) |
|------------|-----|------------|------------|-----|------------|
| 0.1 | 2 | 0.2 | 0.1 | 3 | 0.13 |
| 0.25 | 2 | 0.48 | 0.25 | 3 | 0.32 |
| 0.5 | 2 | 0.95 | 0.5 | 3 | 0.64 |

instantaneous performance degradation can further be reduced by incorporating a beam compressor with a higher m_T as can be realized from Fig. 4(b). As applied to Fig. 3, similar visual analyses of the receivers' tolerance to τ and ξ based on the relatively constant K_s region is also applicable here. For example, it can be seen that $A_F(3, 3) < A_F(3, 5)$ for all detector sizes. Here, $A_F(N, m_T)$ represents the area of the flat (constant K_s) region. Hence, for a given N , a system with a higher m_T demonstrates higher immunity to pointing errors due to vibrations.

In this analysis, we use τ , which is the ratio between the incident angle and the FOV, to compare the performance of different design choices. The receivers' instantaneous FOV (half-angle) can be calculated as $\phi \approx \frac{r_d}{N\zeta d_R}$. Assuming $\zeta \approx 1.0$, the estimated instantaneous ϕ of the receiver designed with the parameters given in Table 1 is given in Table 2.

B. Performance of the Communication Link

The communication link performance for a given aperture size can be characterized by (a) link limited (LL) performance and (b) architecture limited (AL) performance. The LL performance is calculated from the link budget equation that is restrained by communication distance, transmit power, limited receiver optical aperture, etc. The LL performance assumes an optimum receiver design. We calculate the LL lowest achievable BER of the given link to be around 10^{-10} in the absence of pointing jitters that are caused by satellite vibration. However, the performance degrades due to the unavoidable pointing jitters as given in Eqs. (5) and (8). The performance degradation depends on the architecture of the receiver; therefore, architecture-dependent link performance is achieved. The optical architecture of the receiver must be designed carefully to ensure the required BER for seamless data communication. The sample receiver performance of the satellite link in the presence of pointing jitters for different receiver design parameters is shown in Fig. 5. As shown in Figs. 5(a) and 5(b), considering random angular pointing jitters of $0.25 \mu\text{rad} \leq \sigma_T \leq 0.75 \mu\text{rad}$ and $\xi = 0.2$, the LL BER for the given link BER_{LL} is calculated as $10^{-10.7} \leq \text{BER}_{\text{LL}} \leq 10^{-8}$.

Figure 5 also shows that the achievable AL BER [calculated from Eq. (8)] varies notably depending on r_d , m_T , N , and τ . Figure 5(a) presents the impact of pointing jitter on the achievable BER at $\tau = 0.5$. For instance, the achievable BER varies between about $10^{-7.5}$ and $10^{-5.6}$ when a 0.1 mm detector, a 5x beam compressor, and a FL of $N = 2.0$ are incorporated in the sample receiver architecture (as shown in Fig. 2). It can be realized that the AL performance can be improved by implementing a receiver with larger r_d , higher m_T , and larger N (limited by the lens design parameters and available volume). The selection of r_d depends on the communication bandwidth, wavelength, and noise equivalent power (NEP). Frequently, these criteria will limit the options. The bandwidth (BW) of the detector is

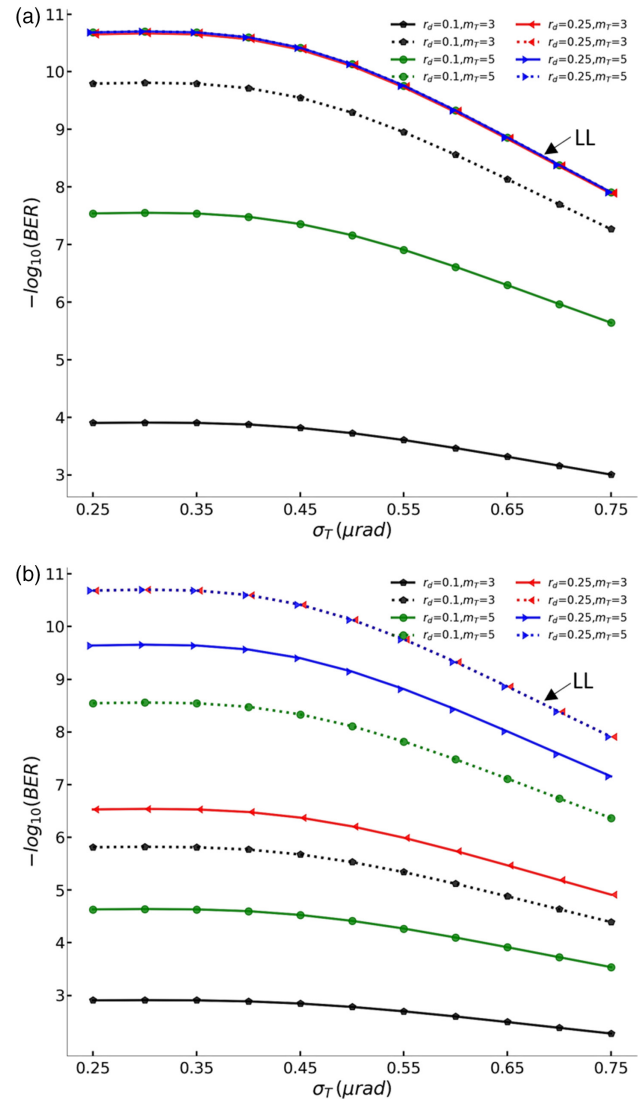


Fig. 5. BER versus σ_T for different m_T and r_d . Solid curves correspond to $N = 2.0$, whereas dashed curves correspond to $N = 3.0$. (a) $\tau = 0.5$; (b) $\tau = 0.75$.

inversely proportional to the detector size, $\text{BW} \propto 1/r_d$. In addition, in many detectors such as PIN photodiodes, $\text{NEP} \propto r_d$ [25,26]. Even though the NEP of most PIN photodiodes increases with the size of the detectors, many communication detectors show opposite behavior, especially avalanche photodiode (APD). For example, two commercially available InGaAs APDs with a diameter of 0.2 mm and 75 μm have NEP of $0.45 \text{ pW}/\sqrt{\text{Hz}}$ and $1.1 \text{ pW}/\sqrt{\text{Hz}}$, respectively [27]. Similarly, 1.0 mm, 0.5 mm, and 0.2 mm Si APDs show $2.5 \text{ fW}/\sqrt{\text{Hz}}$, $0.09 \text{ pW}/\sqrt{\text{Hz}}$, and $0.15 \text{ pW}/\sqrt{\text{Hz}}$ NEP respectively. As a result, the performance gap between 0.1 mm and 0.25 mm as shown in Figs. 5 and 6 may decrease or increase slightly based on the detector types and integrated bandwidth. We assume almost constant NEP for both detectors, and the integrated receiver's bandwidth is fixed at 1.0 GHz by electrical filters. This allows us to compare different receiver designs effectively based on the pointing error.

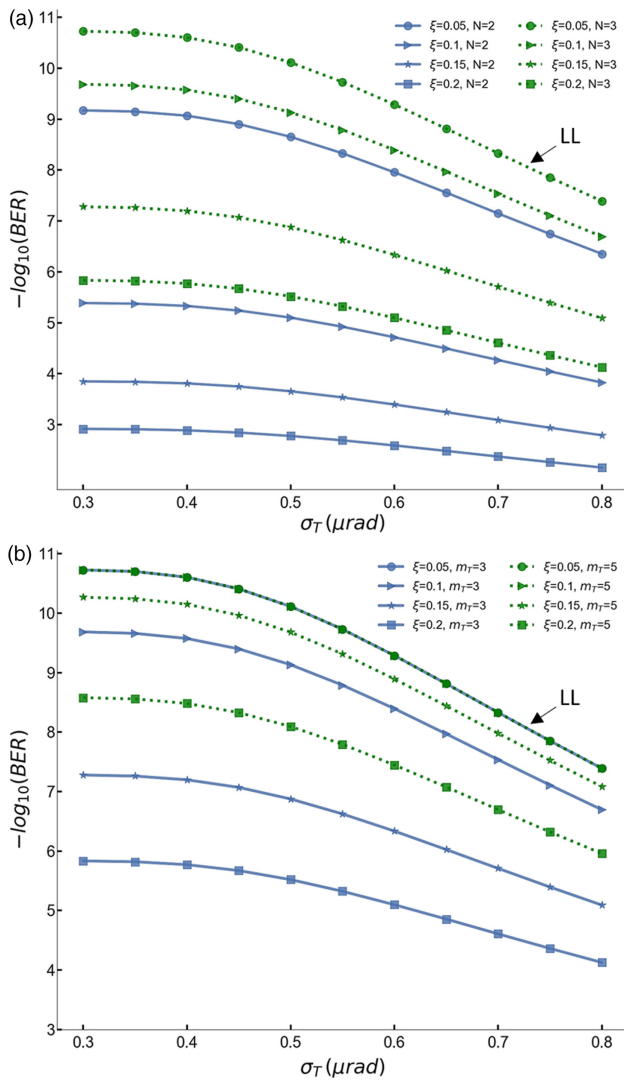


Fig. 6. Dependence of BER on ξ . (a) Effect of different N at $m_T = 3.0$; (b) effect of different m_T at $N = 3.0$.

The LL performance is achievable with certain sets of parameters, e.g., $\{r_d = 0.1, m_T = 5, N = 3\}$ and $\{r_d = 0.25, m_T = 5, N = 3\}$. The effect of receiver architecture is more prominent for a larger AOI as shown in Fig. 5(b). For instance, the same receiver architecture ($r_d = 0.1$ mm, $m_T = 5$, and $N = 2$) shows significantly poor BER, $10^{-4.6} \leq \text{BER} \leq 10^{-3.5}$, at $\tau = 0.75$. However, the LL performance is still achievable with $\{r_d = 0.25, m_T = 3, N = 3\}$ and $\{r_d = 0.25, m_T = 5, N = 3\}$. Consequently, an optimal design parameters set $\{r_d, m_T, N\}$ must be chosen to achieve better link performance over a wide variation of τ in the presence of pointing errors.

Alongside the parameter selection, an optimum optical design that reduces the optical aberrations is also necessary to improve the performance of the satellite optical links as shown in Fig. 6. Figure 6(a) presents the achievable BER for different aberration factor ξ , $0.05 \leq \xi \leq 0.2$ at $m_T = 3.0$. It can be realized that an optical receiver design with low ξ facilitates stable ISOL even at large τ (e.g., $\tau = 0.75$) in the presence of pointing error. For example, considering the sample receiver

architecture as shown in Fig. 2 that incorporates $m_T = 3.0$ and $N = 2.0$, numerical analysis shows that about 6 orders of magnitude ($\approx 10^6$) BER performance improvement is attainable by lowering ξ from 0.2 to 0.05 at low jitter scenario, $\sigma = 0.3 \mu\text{rad}$. Similarly, in the high pointing jitter scenario, $\sigma = 0.8 \mu\text{rad}$, about 10^4 times BER performance improvement is achievable by lowering ξ from 0.2 to 0.05 as shown in Fig. 6(a). Indeed, a low ξ mandates superior optics, complex optical design, higher cost, higher mass, and larger volume. Hence, there is an inevitable trade-off among size, weight, cost, and performance. The performance can be improved by increasing N of the FL while keeping the beam compression ratio unchanged, $m_T = 3.0$. For example, at $\sigma = 0.8 \mu\text{rad}$ and $\xi = 0.15$, the calculated BERs are about 1.6×10^{-3} and 8×10^{-6} for $N = 2.0$ and $N = 3.0$, respectively. Further performance optimization is possible by increasing m_T as shown in Fig. 6(b). For instance, in the low jitter case ($\sigma = 0.3 \mu\text{rad}$), the achievable BER of a receiver that incorporates $N = 3.0$ and $\xi = 0.2$ can be improved to 2.6×10^{-3} ($\approx 10^{-8.6}$) from 1.5×10^{-6} ($\approx 10^{-5.8}$) by increasing m_T from 3.0 to 5.0.

Figure 7 presents the performance space of the sample receiver architecture with a given beam compression ratio and f -number of the FL system while assuming a detector radius of 0.1 mm. The solid curves represent the best-case BER for given m_T and N , whereas the dashed curves present the worst-case performance. Based on the optical design, lens selection, and aberration compensations, different BER curves are achievable that depend on jitter amplitude σ . However, the performance will be bounded by the solid and dashed curves as shown in Fig. 7. One can realize the receiver's immunity to vibration jitters and AOI by analyzing the performance space. For example, the best-case BER of the system that incorporates $m_T = 3.0$ and $N = 2.0$ as shown in Fig. 7(a) starts rolling off around $\tau = 0.7$, and the worst-case performance fails to establish error-free communication [considering forward error correction (FEC)] when

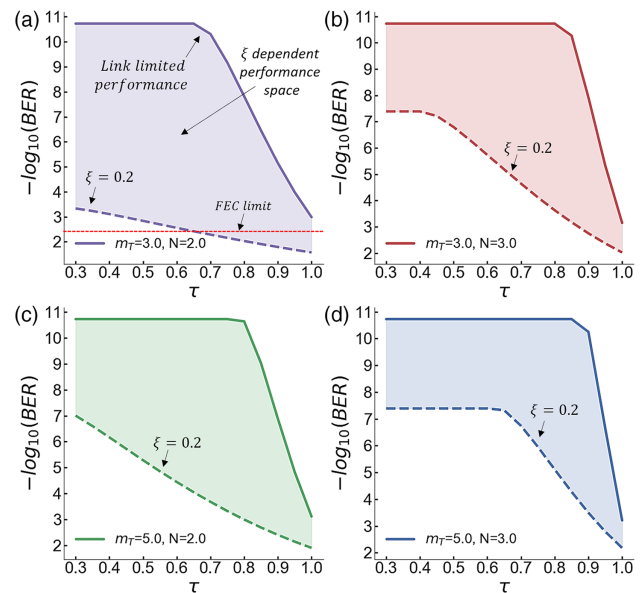


Fig. 7. Performance limit of the sample receiver architecture with a 0.1 mm detector for given m_T and N . (a) $m_T = 3.0, N = 2.0$; (b) $m_T = 3.0, N = 3.0$; (c) $m_T = 5.0, N = 2.0$; (d) $m_T = 5.0, N = 3.0$.

$\tau \geq 0.65$. On the contrary, it can be seen from Fig. 7(d) that if the receiver system is designed with $m_T = 5.0$ and $N = 3.0$, the best-case BER and the worst-case BER are immune to the variation of σ and τ up to $\tau \approx 0.9$ and $\tau \approx 0.68$. A similar analysis of the performance roll-off can be done with Figs. 7(b) and 7(c). It is evident that $BER_{3-2} < BER_{5-2} < BER_{3-3} < BER_{5-3}$, where BER_{m_T-N} denotes the overall expected communication performance based on BER for given m_T and N in the presence of pointing jitters caused by satellite vibrations. We can notice that a receiver design with a larger N (for a given m_T) as well as a higher m_T (for a given N) is expected to perform better over a wider AOI in the presence of jitters as can be seen from Fig. 7. The above-mentioned analyses assume a 100 km communication distance with link parameters given in Table 1. An optimum optical receiver can be designed for a given satellite platform and communication requirement by analyzing major design parameters of the architecture as presented in this manuscript.

4. CONCLUSION

In summary, in this paper, we present an analytical model to estimate the impact of optical receiver design parameters on the ISOL in the presence of angular pointing jitters. As a case study, we present the effect of receiver design parameters on a direct detection CubeSat optical link to demonstrate the receiver design techniques with high pointing jitter rejection. Our study points out that a well-engineered optical receiver can have significant tolerance to random pointing errors that are originated from the satellite vibration and noise in the sensor systems. The analyses carried out here can be the basis for optimum optical receiver design to achieve the best ISOL performance.

Funding. Office of Naval Research (N00014-18-1-2845).

Disclosures. The authors declare no conflicts of interest.

REFERENCES

- J. E. Velazco, J. Griffin, D. Wernicke, J. Huleis, A. DeNucci, O. Boyraz, and I. U. Zaman, "Inter-satellite omnidirectional optical communication for remote sensing," *Proc. SPIE* **10769**, 157–162 (2018).
- K. Cahoy, P. Grenfell, A. Crews, M. Long, P. Serra, A. Nguyen, R. Fitzgerald, C. Haughwout, R. Diez, A. Aguilar, J. Conklin, C. Payne, J. Kusters, C. Sackier, M. LaRocca, and L. Yenchesky, "The CubeSat Laser Infrared Crosslink mission (CLICK)," *Proc. SPIE* **11180**, 358–369 (2019).
- I. U. Zaman, A. W. Janzen, R. Torun, J. E. Velazco, and O. Boyraz, "Design tradeoffs and challenges of omnidirectional optical antenna for high speed, long range Inter CubeSat data communication," in *Small Satellite Conference, Delivering Mission Success (SSC18-WKII-06)* (2018).
- I. U. Zaman, J. E. Velazco, and O. Boyraz, "Realization of omnidirectional CubeSat crosslink by wavelength-selective optical transceiver," *IEEE J. Miniatur. Air Space Syst.* **1**, 47–55 (2020).
- J. E. Velazco, J. Griffin, A. W. Janzen, J. Huleis, M. Peng, A. DeNucci, I. U. Zaman, and O. Boyraz, "High data rate inter-satellite omnidirectional optical communicator," in *32nd Annual AIAA/USU Conference on Small Satellites* (2018), paper SSC18-WKI-02.
- J. Ma, X. Li, S. Yu, L. Tan, and Q. Han, "Influence of satellite vibration on optical communication performance for intersatellite laser links," *Opt. Rev.* **19**, 25–28 (2012).
- M. E. Wittig, L. V. Holtz, D. E. L. Tunbridge, and H. C. Vermeulen, "In-orbit measurements of microaccelerations of ESA's communication satellite Olympus," *Proc. SPIE* **1218**, 205–214 (1990).
- F. Sansone, A. Francesconi, R. Corvaja, G. Vallone, R. Antonello, F. Branz, and P. Villorosi, "LaserCube optical communication terminal for nano and micro satellites," *Acta Astronaut.* **173**, 310–319 (2020).
- S. Arnon, S. R. Rotman, and N. S. Kopeika, "Performance limitations of free-space optical communication satellite networks due to vibrations: direct-detection digital mode," *Proc. SPIE* **3110**, 357–368 (1997).
- S. Arnon and N. S. Kopeika, "The performance limitations of free space optical communication satellite networks due to vibrations-analog case," in *19th Convention of Electrical and Electronics Engineers in Israel* (1996), pp. 287–290.
- C.-C. Chen and C. Gardner, "Impact of random pointing and tracking errors on the design of coherent and incoherent optical intersatellite communication links," *IEEE Trans. Commun.* **37**, 252–260 (1989).
- J. D. Barry and G. S. Mecherle, "Beam pointing error as a significant design parameter for satellite-borne, free-space optical communication systems," *Opt. Eng.* **24**, 1049–1054 (1985).
- T. Song, Q. Wang, M.-W. Wu, T. Ohtsuki, M. Gurusamy, and P.-Y. Kam, "Impact of pointing errors on the error performance of intersatellite laser communications," *J. Lightwave Technol.* **35**, 3082–3091 (2017).
- S. G. Lambert and W. L. Casey, *Laser Communications in Space* (Artech House, 1995).
- S. Arnon, S. Rotman, and N. S. Kopeika, "Beam width and transmitter power adaptive to tracking system performance for free-space optical communication," *Appl. Opt.* **36**, 6095–6101 (1997).
- M. Scheinfeild, N. S. Kopeika, and R. Melamed, "Acquisition system for microsatellites laser communication in space," *Proc. SPIE* **3932**, 166–175 (2000).
- J. Chang, C. M. Schieler, K. M. Riesing, J. W. Burnside, K. Aquino, and B. S. Robinson, "Body pointing, acquisition and tracking for small satellite laser communication," *Proc. SPIE* **10910**, 144–152 (2019).
- M. Guelman, A. Kogan, A. Kazarian, A. Livne, M. Orenstein, and H. Michalik, "Acquisition and pointing control for inter-satellite laser communications," *IEEE Trans. Aerosp. Electron. Syst.* **40**, 1239–1248 (2004).
- H. Liu, Y. Tian, F. L. Lewis, Y. Wan, and K. P. Valavanis, "Robust formation flying control for a team of satellites subject to nonlinearities and uncertainties," *Aerospace Sci. Technol.* **95**, 105455 (2019).
- H. T. Friis, "A note on a simple transmission formula," *Proc. IRE* **34**, 254–256 (1946).
- G. P. Agrawal, *Fiber-Optic Communication Systems*, 3rd ed. (Wiley, 2004), pp. 162–167.
- R. W. Kingsbury, "Optical communications for small satellites," Ph.D. thesis (Massachusetts Institute of Technology, 2015).
- M. Toyoshima, "Trends in satellite communications and the role of optical free-space communications [Invited]," *J. Opt. Netw.* **4**, 300–311 (2005).
- I. U. Zaman, J. E. Velazco, and O. Boyraz, "Omnidirectional optical crosslinks for CubeSats: transmitter optimization," *IEEE Trans. Aerospace Electron. Syst.* (2020).
- HAMAMATSU, "Characteristics and use of infrared detectors," 2004, <https://mmrc.caltech.edu/FTIR/Literature/General/Hamamatus%20IR%20detectors.pdf>.
- Thorlabs, "Photodiodes," 2020, https://www.thorlabs.com/newgroup/page9.cfm?objectgroup_id=285.
- Thorlabs, "InGaAs Avalanche Photodetectors/Photodiodes," 2020, https://www.thorlabs.com/newgroup/page9.cfm?objectgroup_id=4047.